Journal of Applied Research and Technology

www.jart.icat.unam.mx

Journal of Applied Research and Technology 21 (2023) 407-423

Original

An intermediate water gravity wavelength and wave height measurement inside a large wave flume tank

Safa M. Aldarabseh[a]* • Parviz Merati[b]

[a]*Department of Mechanical Engineering, Tafila Technical University, Tafila*
[b]*Department of Mechanical and Aerospace Engineering, Western Michigan University, USA.*

Received 08 29 2021; accepted 02 03 2022
Available 06 30 2023

Abstract: This paper discusses the performance of three methods to measure the intermediate water gravity wavelength and wave height. Three methods were used to obtain wave height, wavelength, and period. Firstly, conventional methods used two Honeywell pressure sensors mounted at the bottom of the wave tank at two different locations. Secondly, use the transfer function of the flap wavemaker (the relationship between wave height and the wave paddle stroke). Thirdly, the image-based method by analyzing images captured using the PIV technique. The significant wave height and period from pressure reading sensors of regular gravity waves were obtained from the Raleigh distribution and zero-up crossing technique. Wavelength was obtained indirectly by using a dispersion relationship that was solved by using the Newton Raphson numerical method from both the pressure sensors and the transfer function of the flap wavemaker. This paper shows the novel technique to obtain the direct value of wavelength and wave height by analyzing PIV images to replace the conventional methods and eliminate the error that may produce by using the numerical methods. The PIV setup with the CCD camera was used to capture wave images. The image processing technique based on Canny edge detection with constant threshold value was used to detect the edge of the waves. The maximum and minimum points of the detected edges of the waves were obtained using Matlab code, and then wavelength and wave height can be obtained directly from these images that were considered as the true value of the wave measurements. The results showed that the accurate value of wavelength and wave height obtained based on the pressure measurements and wavemaker transfer function are strongly dependent on the numerical method that should be used to solve the dispersion theory.

Keywords: Wave flume tank, Flap wavemaker, Stroke, Honeywell pressure sensors, PIV image processing technique

*Corresponding author.
E-mail address: Aldarabsehsafaa@gmail.com (Safa M. Aldarabseh).
Peer Review under the responsibility of Universidad Nacional Autónoma de México.

1. Introduction

this study). Most of these methods are intrusive, expensive, complicated, and point measurement methods. Meaning if you are looking to measure wave parameters at a different location along the water surface or to obtain the spatial change in water surface elevation, a huge number of sensors or gauges should be used. These gauges must be calibrated with specific equipment to get the desired accuracy. Also, these gauges are in direct contact with the flow field means the flow field disturbance is frequently unavoidable (Hernández et al., 2018; Liu et al., 1982; Lee & Wang, 1984; Yao & Wu, 2005). Optical sensors (Blenkinsopp et al., 2012; Li et al., 1993; Payne et al., 2009), ultrasonic sensors (Blenkinsopp et al., 2010; Vousdoukas et al., 2014) have been used to evaluate the water surface elevation. To overcome the limitations of the intrusive methods, nonintrusive image-based techniques have been developed to obtain the water surface elevation (Douglas et al., 2020; Escudero et al., 2021; Hernández-Fontes et al., 2020; Hernández et al., 2018; Iglesias et al., 2009; Yao & Wu, 2005).

Study (Siddiqui et al., 2001) used a PIV technique with a CCD video camera that was mounted above the water surface, and it is looking down at an angle of 34° from the horizontal axis to estimate the water surface elevation. The constant threshold value that was calculated based on the average grayscale value below the water surface was used to detect water surface elevation. In Hwung et al. (2009) water surface elevation obtained by using a CCD camera that was mounted above the water surface with three different angles from the horizontal axis. They detected water surface elevation using two detection algorithms, which were the hyperbolic tangent function (HTF) and threshold method (TM). In Mukto et al. (2007) a DPIV technique was used with a CCD camera that was mounted above the water surface, and it is looking down at an angle of 11° from the horizontal axis to estimate the water surface elevation. Water surface elevation was detected by the edge detection algorithm based on the variable threshold method. In Bonmarin et al. (1989) a visualization technique was used to perform a wave profile. This technique required a visible water surface under a given illumination, and this was done by using a thin sheet of light to illuminate fluorescein that was put in the flume tank. In their experiment the CCD video camera was placed in front of a flume tank to record the wave profile. Water surface elevation was detected by converting the digital image (signal) to a binary image (digital) that was done by applying an operator-adjustable threshold level. In Wang et al. (2012) integrated the modified plane-based camera calibration (MPCC) with an inexpensive internet web camera as the imaging device to measure water surface elevation. In Yao and Wu (2005) the DPIV technique was used with a CCD camera to detect water surface elevation. Wave profile was detected using a gradient vector flow active contour model (GVF) snake. In Erikson and Hanson (2005) a CCD video camera was used to measure wave profile. To form a visible video under a given illumination, the uniform light source was used to illuminate fluorescent green dye that was put inside the flume tank. Then they transferred the digital data from the camcorder to the computer using a high-speed interface. Surface water elevation was detected by employing the Matlab's edge command (Robert's edge detector) in the signal processing toolbox. In Zarruk (2005) particle image velocimetry (PIV) was used with a CCD camera to detect water surface elevation using the location of the maximum intensity gradient. The Bonferroni coefficient was used to detect the location of the maximum intensity gradient. In Viriyakijja and Chinnarasri (2015) two CCD video cameras were used and mounted perpendicular to the flume tank. They used canny edge detection to detect water surface elevation. They used a zero-up crossing method to obtain wave height and wave period. Then they solved dispersion relation with Hunt's equation to obtain wavelength. Also, by using these methods relationship between time(frequency) and change in water surface elevation was produced, then wave height and period could be found by Rayleigh distribution or zero up crossing methods. The wavelength could be obtained by solving dispersion relation with one of the numerical methods that were explained later in this paper. Thus, significant errors could be found by using numerical methods to get wavelength. Up to the author's knowledge wavelength was evaluated indirectly by getting the value of wave height and frequency, and then using numerical methods to get wavelength. The current study was focused on getting the direct value of wavelength and eliminating the errors that may produce by solving dispersion relation theory by one of the numerical methods. All the above-mentioned literature compared their results with results obtained from conventional methods (capacitance wave gauges or pressure sensor) for verification. In this study, the PIV technique was used to capture the image for the water gravity waves at different frequencies. Then these images were analyzed by using the edge detection algorithm that was built using Matlab to get wavelength and wave height experimentally and these values are considered as the true value of wave measurements. Then, compared with the values obtained from the theoretical method (flap wavemaker transfer function theory) and conventional method (pressure measurement). Thus, the main objective of this study is to measure the performance of these three methods to measure the intermediate water gravity wavelength and wave height. While the wave period (frequency) is easy to get, as explained later, by using a digital photosensor tachometer, or can be considered as the time required for the 100-wave crests to pass a fixed point at 2 m far away from the wavemaker, using a stopwatch (Saincher & Banerjee, 2015)

2. Experimental setup and measurements

2.1. Experimental setup

This experiment focused on the intermediate water gravity waves $\left(\frac{h}{L} = 0.15693, 0.35816, 0.47487\right)$. In this study, these waves were produced by using a mechanical force such as a motor-driven paddle at one side of a flume tank. The amplitude and frequency of the paddle can be controlled in the paddle drive system. The experiment detailed in this study was carried out in a wave tank at the fluid dynamic laboratory at Western Michigan University. The wave flume tank consists of a clear acrylic plexiglass channel with dimensions 7.32 m long, 0.15 m wide, and 0.36 m deep. The flume tank was divided into three equal sections, and the middle section was the test section. The schematic diagram of the wave flume tank can be seen in Figure 1.

2.2. Wave parameter measurements

Mechanically driven wavemaker made of plexiglass hinged at the bottom of the flume tank with adjustable wave amplitude and wave frequency that produce sinusoidal wave motion. The electrical motor wave generator that was used to drive the Plexiglas flap wavemaker is composed of a ¼ HP, maximum 1725 RPM, 115 V, and 4.4 A. Electrical motor and a Plexiglas flap, see Figure 2.

Waves were generated by a flap-type bottom-hinged paddle mounted at one end of the tank, which travels down the trough and is employed to dissipate smoothly on the slope of the beach, or it can be called a wave absorber, as seen in Figure 1. The paddle (wavemaker) was driven by an electrical motor. Various paddle motion was achieved by varying the rotational speed of the electrical motor.

Three methods were used to obtain wave height, wavelength, and period. Firstly, Honeywell pressure sensors were mounted at the bottom of the wave tank at two different locations: one at 1 m from the wavemaker (PS1) and the other at 5 m from the wavemaker (PS2) to get a fully developed wave, as shown in Figure 1. Wave height and period were obtained from pressure reading, and then the linear wave theory equation was implemented, especially dispersion relation to getting wavelength. Secondly, analyzed PIV images to obtain the values of wave height and wavelength. Finally, by assuming that the frequency of the wavemaker is the same as wave frequency, then the dispersion relation could be used to get wavelength and then use the transfer function of the flap wavemaker (the relationship between wave height and the wave paddle stroke) to get wave height.

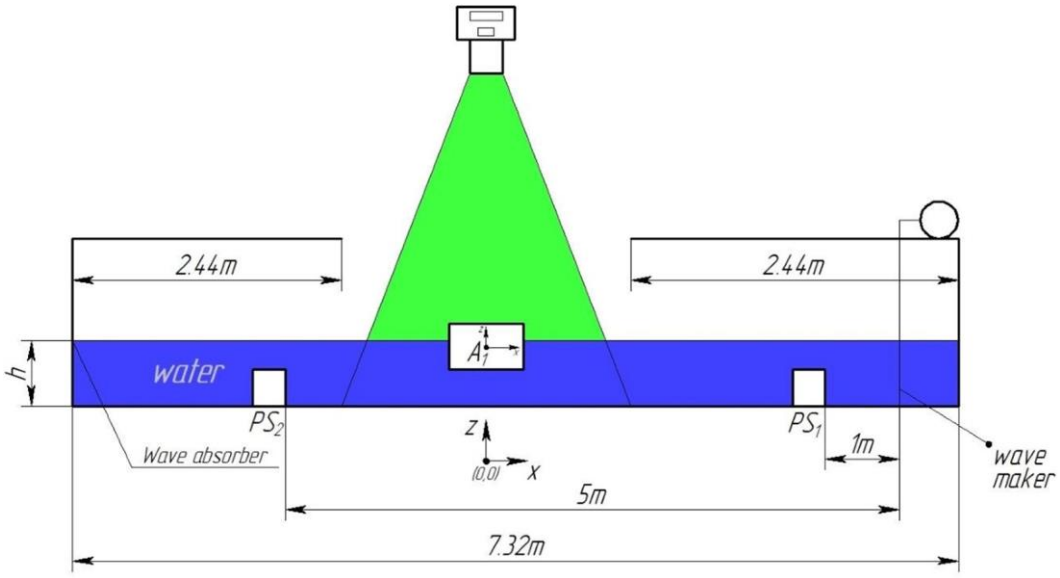

Figure 1. Schematic diagram of the wave flume tank setup. PS1 & PS2 are denoted as the locations of the Honeywell pressure sensors mounted at the bottom of the wave flume tank. A1 is denoted as the test section at the water surface level, and h= 17 cm is denoted as the still water level.

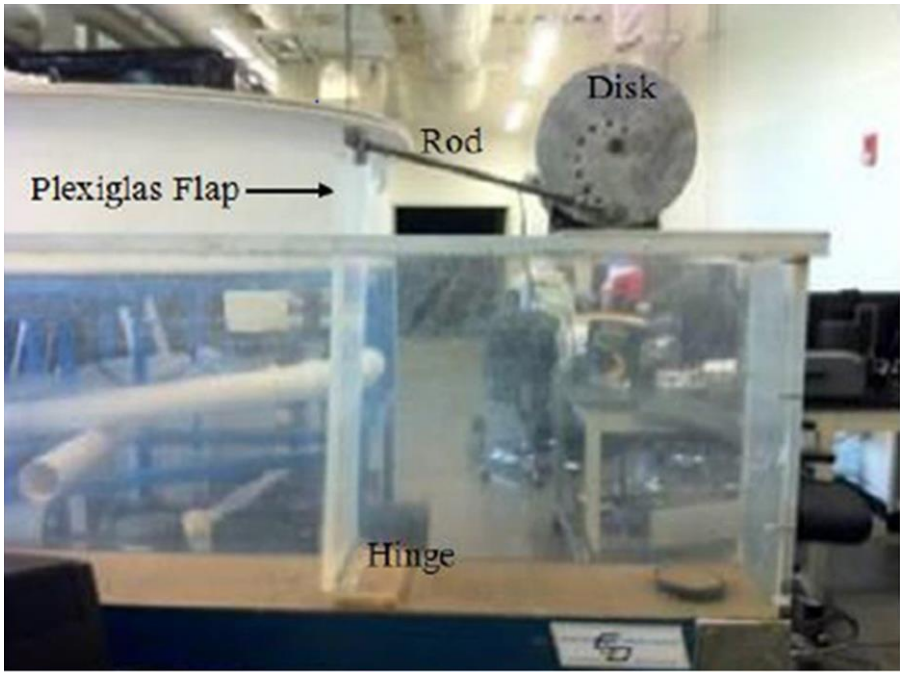

Figure 2. Schematic diagram of the wave generator system.

3. Mathematical modeling

3.1. Wave characteristics

Four parameters define characteristics of the gravity wave that are: height (H, m) or amplitude (a=H/2, m), length (L, m), period (T, sec) or angular wave frequency (ϖ, 1/sec), and wave steepness (H/L) or this parameter (H/T, m/sec). Wave height is the vertical distance between the crest and the trough. The amplitude is the distance from the still water level, also known as zero energy level (assumed to be at the center of the wave is the halfway between the crest and trough, h(m)), to the bottom of the trough or the top of the crest. Thus, the wave height is twice the wave amplitude. Wavelength is the horizontal distance between two successive troughs or crests. The wave period is the time required for one full wavelength to pass a given point. Where the wave frequency is the number of a wave crest or wave trough that passes a fixed point per unit of time and is the inverse of the period. Wave steepness is the ratio between wave height and wavelength, see Figure 3.

Wind waves are classified according to the ratio between still water depth and wavelength (h/L). Thus, wind waves are considered as deep-water waves when the still water depth is greater than half of the wavelength $\left(h > \frac{L}{2}\ or \frac{h}{L} > 0.5\right)$, intermediate or transitional water waves when $\left(\frac{L}{2} > h > \frac{L}{20}\ or\ 0.5 > \frac{h}{L} > 0.05\right)$, and shallow water waves when $(h > \frac{L}{2}\ or \frac{h}{L} > 0.5)$This study was concerned with intermediate water gravity waves (0.15693, 0.35816, 0.47487).

3.2. Linear gravity wave theory

Linear gravity wave theory, also known as the Airy wave theory, is defined as the most straightforward theory used to obtain equations that provide the kinematic and dynamic properties for a two-dimensional small-amplitude surface gravity wave. The linear wave theory assumes that the ratio of the wave height to wavelength is less than 1/7, which means small wave steepness. The main assumptions for the linear wave theory are as follow:

1- Water is considered as a homogenous and incompressible fluid, and wavelength is greater than 3 cm so that the capillary effect can be neglected.

2- Flow is irrotational; that is no shear stress anywhere at the air-water interface or the bottom of the tank.

3- The bottom of the tank is not moving and is impermeable and horizontal, which means there is no energy transfer through the bottom.

4- The pressure along the air-water interface is constant; that means there is no effect of wind on the pressure difference between maximum at crest and minimum at the trough.

The most important assumption is the wave amplitude is small compared to the wave height and still water level.

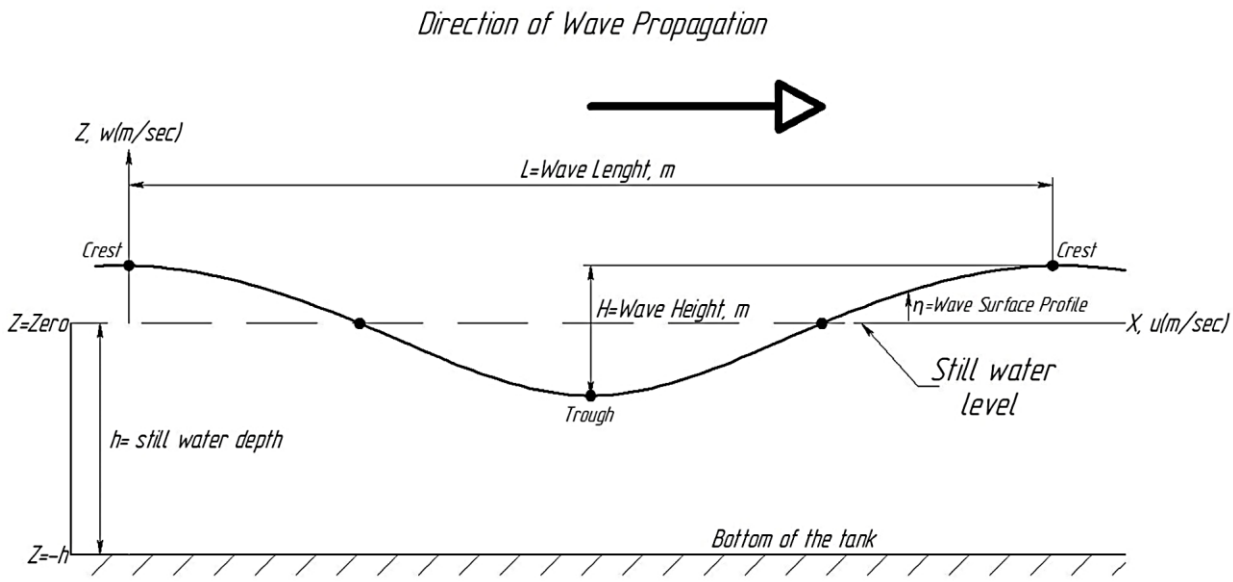

Figure 3. The wave of water parameters.

3.2.1. Governing equations

1- Navier – stokes equation, as shown in Eq.1

$$\rho\frac{\partial}{\partial t}(u_j)+\rho u_k\frac{\partial}{\partial x_k}(u_j)=-\frac{\partial P}{\partial x_j}+\mu\frac{\partial^2}{\partial x_i\,\partial x_i}(u_j)+\rho f_j \quad (1)$$

Where

$\rho\ \left(\frac{Kg}{m^3}\right)$ water density. $U, w\ \left(\frac{m}{sec}\right)$ water surface velocity in x and z direction, respectively.

By ignoring the viscous force and expanding the above equation into two considered directions (x, z), the following two Euler equations are derived, respectively, as shown in Eq. 2 and 3:

$$\frac{\partial u}{\partial t}+u\frac{\partial u}{\partial x}+w\frac{\partial u}{\partial z}=-\frac{1}{\rho}\frac{\partial P}{\partial x} \quad (2)$$

$$\frac{\partial w}{\partial t}+u\frac{\partial w}{\partial x}+w\frac{\partial w}{\partial z}=-\frac{1}{\rho}\frac{\partial P}{\partial z}+g \quad (3)$$

2- Continuity equation, as shown in Eq. 4

$$\frac{\partial u}{\partial x}+\frac{\partial w}{\partial z}=\text{zero} \quad (4)$$

Introduce the velocity potential function $\phi(x,t)$, as $\left(u=\frac{\partial\phi}{\partial x},\ \ w=\frac{\partial\phi}{\partial z}\right)$ then substitute two of these formulas back into Eq. 2, 3, and 4, becomes as shown in Eq. 5 and 6

$$\frac{\partial^2\phi}{\partial t\,\partial x}+\frac{\partial\phi}{\partial x}\frac{\partial^2\phi}{\partial x^2}+\frac{\partial\phi}{\partial z}\frac{\partial^2\phi}{\partial z\,\partial x}=\frac{-1}{\rho}\frac{\partial P}{\partial x} \quad x-\text{direction} \quad (5)$$

$$\frac{\partial^2\phi}{\partial t\,\partial z}+\frac{\partial\phi}{\partial x}\frac{\partial^2\phi}{\partial x\,\partial z}+\frac{\partial\phi}{\partial z}\frac{\partial^2\phi}{\partial z^2}=\frac{-1}{\rho}\frac{\partial P}{\partial z}+g \quad z-\text{direction} \quad (6)$$

Integrate the above equation on (x, z) directions, respectively; the following Eq. 7 and 8 are obtained:

$$P+\rho\frac{\partial\phi}{\partial t}+\frac{1}{2}\rho(u^2+w^2)=C \quad x-\text{direction} \quad (7)$$

$$P+\rho\frac{\partial\phi}{\partial t}+\frac{1}{2}\rho(u^2+w^2)+\rho gz=C \quad z-\text{direction} \quad (8)$$

As shown above, the two force equations are precisely the same, but the second equation includes gravity effects. Therefore, a single equation for the whole field was developed

and is known as the Bernoulli equation for unsteady irrotational flow, as shown in Eq. 9.

$$P + \rho\frac{\partial\phi}{\partial t} + \frac{1}{2}\rho(u^2 + w^2) + \rho g z = C \tag{9}$$

The continuity equation is transformed to the Laplace equation as follows in Eq. 10:

$$\frac{\partial^2\phi}{\partial x^2} + \frac{\partial^2\phi}{\partial z^2} = \text{zero} \tag{10}$$

Defined Boundary conditions as follows:

1. The kinematic boundary conditions at the bottom of the wave tank. Based on the previous assumption, we assumed the bottom of the wave tank is not moving, as shown in Eq. 11.

$$w = \frac{\partial\phi}{\partial z} = \text{zero} \quad \text{at} \quad (z = -h) \tag{11}$$

2. The boundary condition at the water-free surface

a- Kinematic boundary condition related to the vertical velocity at the water-free surface, as shown in Eq. 12.

$$w = \frac{\partial\eta}{\partial t} + u\frac{\partial\eta}{\partial x} \quad \text{at} \quad (z = \eta) \tag{12}$$

b- Dynamic boundary condition related to the pressure at the water-free surface, as shown in Eq. 13

$$\rho\frac{\partial\phi}{\partial t} + \frac{1}{2}\rho(u^2 + w^2) + \rho g z = \text{zero} \quad \text{at} \quad (z = \eta) \tag{13}$$

The boundary condition at free water surface must be linearized and reapplied at still water level $(z = \text{zero})$ instead of $(z = \eta)$. This developed Eq. 14 and 15

$$w = \frac{\partial\eta}{\partial t} \quad \text{at} \quad (z = \text{zero}) \tag{14}$$

$$\frac{\partial\phi}{\partial t} + g\eta = \text{zero} \quad \text{at} \quad (z = \text{zero}) \tag{15}$$

Velocity potential function (ϕ) for small-amplitude surface gravity wave was derived by solving the LaPlace Eq. 10 using kinematic boundary condition at the bottom and the linearized dynamic boundary condition at the free water surface, as shown in Eq. 16.

$$\phi = \frac{g a}{\omega}\frac{\cosh k(h + z)}{\cosh(kh)}\sin(kx - \omega t) \tag{16}$$

$$\text{where wavenumber } (k) = \frac{2\pi}{L}$$

Wave surface profile (η) was derived by inserting the velocity potential function into a linearized dynamic boundary condition, as shown in Eq. 17.

$$\eta = \frac{H}{2}\cos(kx - \omega t) \tag{17}$$

The dispersion relation is known as the relationship between the wave frequency and wavenumber at a given still water depth. It was derived by adding the two linearized boundary conditions at the free water surface (dynamic and kinematic) together, then applying velocity potential and differentiating. This yield Eq. 18.

$$\omega = \sqrt{gk\tanh(kh)} \tag{18}$$

3.3. Pressure under waves

Pressure under the still water level depends on two factors: hydrostatic pressure due to the depth of still water and the dynamic pressure caused by waves. The pressure at any water level can be obtained by applying the Bernoulli equation for unsteady irrotational flow, as shown in Eq. 19.

$$P = -\rho\frac{\partial\phi}{\partial t} - \frac{1}{2}\rho(u^2 + w^2) - \rho g z \tag{19}$$

Since we are dealing with a linearized condition, the second-order term $(u^2 + w^2)$ must be ignored, then inserting velocity potential function. This yields the following relation, Eq. 20:

$$P = -\rho g z + \frac{\rho g H}{2}\left[\frac{\cosh k(h + z)}{\cosh(kh)}\right]\cos(kx - \omega t) \tag{20}$$

The first term represents hydrostatic pressure, and the second term represents dynamic pressure (wave pressure). See Figure 4.

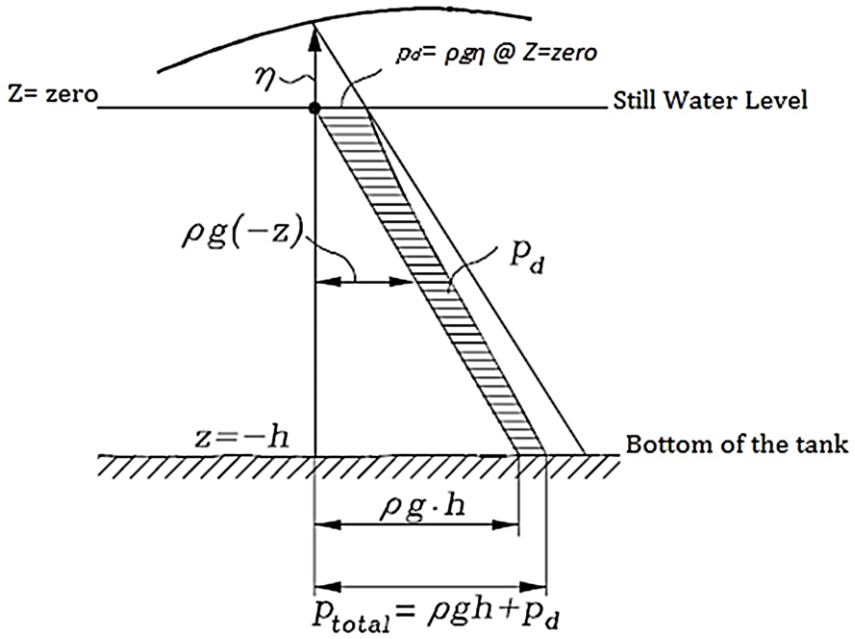

Figure 4. Pressure variation under the wave crest(Andersen & Frigaard, 2011).

4. Methods of measuring wave heights

4.1. Based on the theory of flap wavemaker

There are many ways used to generate regular waves such as piston type, flap (hinged) type, or plunger-type (Dean & Dalrymple, 1991). In the present work, flap (Hinged) type was used to generate regular waves in the wave tank in the fluid dynamics lab at Western Michigan University. Wave paddle stroke is defined as the maximum stroke distance that can be traveled by flap wavemaker at the free water surface (S, cm). The stroke of the flap was adjusted from 5.43 cm at the still water level (17 cm) to 11.5 cm at the top of the wave tank (36 cm), see Figure 5. The flap was attached to the bottom of the wave tank by a hinge that allows the flap wave maker to move forward and backward with the rotation of the electrical motor, as was shown in Figure 2.

Wave frequency, wavelength, and wave height were controlled by adjusting the stroke of the flap wavemaker and the frequency of the electrical motor. A digital photosensor tachometer was used to measure the electrical motor frequency with an accuracy of ±0.05%. To use the theory of flap wavemaker, the frequency of the wave paddle should be the same as the frequency of the wave generated. Thus, wave frequency was also measured by the time required for the 100 wave crests to pass a fixed point at 2 m far away from the wavemaker, using a stopwatch. Many wave crests were selected as the period of waves was up to 0.958 sec. So, it's obvious that human error in measurements would be reduced if the time taken for passage of the 100 wave crests through a specific point were measured as opposed to say, for example, the ten wave crests. Hence, the accuracy in measurements of wave period increase with the number of waves under consideration (Saincher & Banerjee, 2015). The result was very close, and the error between the two readings was between (0.048%, 0.035%, and zero), and that means the results could be used to apply the transfer function of the flap wavemaker, as follows in Eq.21, (Dean & Dalrymple, 1991):

$$\frac{H}{S} = 4\left(\frac{\sinh(kh)}{kh}\right)\frac{kh\sinh(kh) - \cosh(kh) + 1}{\sinh(2kh) + 2kh} \qquad (21)$$

To use the Eq. 21, it should have the value of wavelength first. So, in this method, dispersion theory was used to get wavelength then substituted back into transfer function to get wave height. Thus, the wavelength cannot be directly solved for a given set of wave periods (T) or still water depth(h) from dispersion theory. Therefore, to get the wavelength value, it should be found by iteration. In this study, four numerical methods were used to get wavelength, as explained later.

4.2. Based on pressure measurements

In this study, two Honeywell pressure sensors were used to measure wave height. They were placed one and five meters away from the flap wavemaker. These sensors should not be placed directly at the water medium; thus, these sensors were fixed outside the wave tank and connected with a clear plastic tube, and that tube was tied and fixed at the bottom of the wave tank. These pressure sensors are designed to provide the outcome reading for the pressure. That means the outcome readings must be calibrated to obtain the actual readings of the pressure then turned to wave height by using Rayleigh distribution and zero down crossing method. Firstly, the two Honeywell pressure sensors must be calibrated to connect the measured value and actual pressure reading. The calibration test was done twice for two Honeywell pressure sensors. The calibration test was done by placing the pressure sensor as mentioned above, then changing the depth of still water above the pressure sensor. In the meantime, measured value (outcome from the pressure sensor) was recorded and calculated with the corresponding value of the actual hydrostatic pressure, as follows in Eq. 22:

$$\mathrm{P_{hydrostatic}} = \rho g h \qquad (22)$$

Where ρ is defined as the density of water $1000\frac{Kg}{m^3}$, g is defined as the gravitational acceleration of $9.81\frac{m}{sec^2}$, and h(m) is defined as the depth of still water. The measured values and actual pressure readings at different still water depths are listed in Table 1.

As seen in Figure 6, the correlation coefficient $(R^2\ is\ 0.9797)$ means there is a high correlation between measured and actual value. Thus, the calibration correlation is as follows in Eq. 23:

$$\mathrm{P(m_V)} = 4 * 10^6 * \mathrm{m_V} - 13445 \qquad (23)$$

Where $P(m_V)$ is defined as the actual pressure reading $(Pa)$and $m_V$is defined as the outcome reading from the pressure sensor. After the value of the actual pressure under the waves was evaluated, the pressure value must be converted to wave height by applying the equation of total pressure that was derived above at Z=-h, like the following:

Maximum Pressure reading was measured at the crest at η_{max}, as shown in Eq. 24 :

$$\mathrm{P_{max}} = \rho g h + \frac{\rho g \eta_{max}}{\cosh(kh)} \qquad (24)$$

Minimum Pressure reading was measured at the Trough at η_{min}, as shown in Eq. 25 :

$$\mathrm{P_{min}} = \rho g h + \frac{\rho g \eta_{min}}{\cosh(kh)} \qquad (25)$$

Wave height is the difference between the maximum and minimum wave surface elevation

$(\eta_{max} - \eta_{min})$, shown in Figure 7.

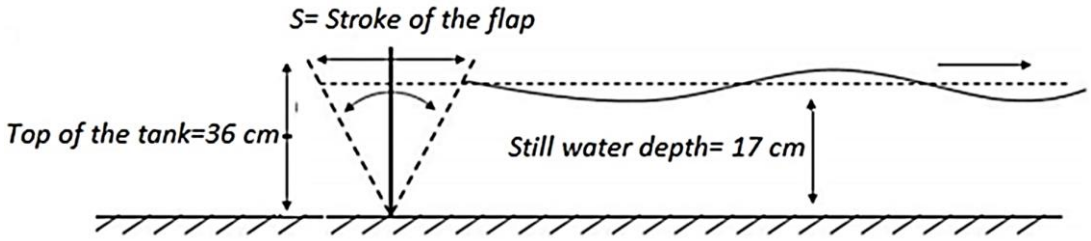

Figure 5. Schematic diagram of paddle flap wavemaker.

Table 1. Hydrostatic pressure and corresponding outcome of pressure sensor at different still water depths.

Still Water Depth(m)	Measured Value (m_V)	Actual Hydrostatic Pressure (P, Pa)
0.1725	0.00358579	1692.225
0.123	0.003499	1206.63
0.1	0.003402	981
0.07	0.003326	686.7
0.05	0.003320	490.5
0	0.00320	0

The information in the table above allows us to draw a relation between measured and actual reading to get a calibration correlation, as shown in Figure 6.

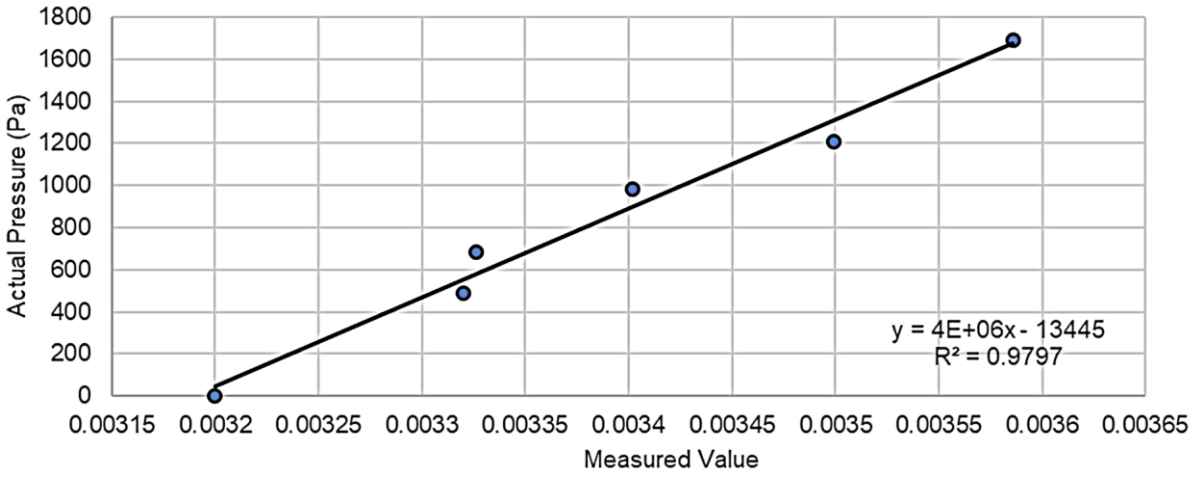

Figure 6. Calibration correlation between a measured value and actual value.

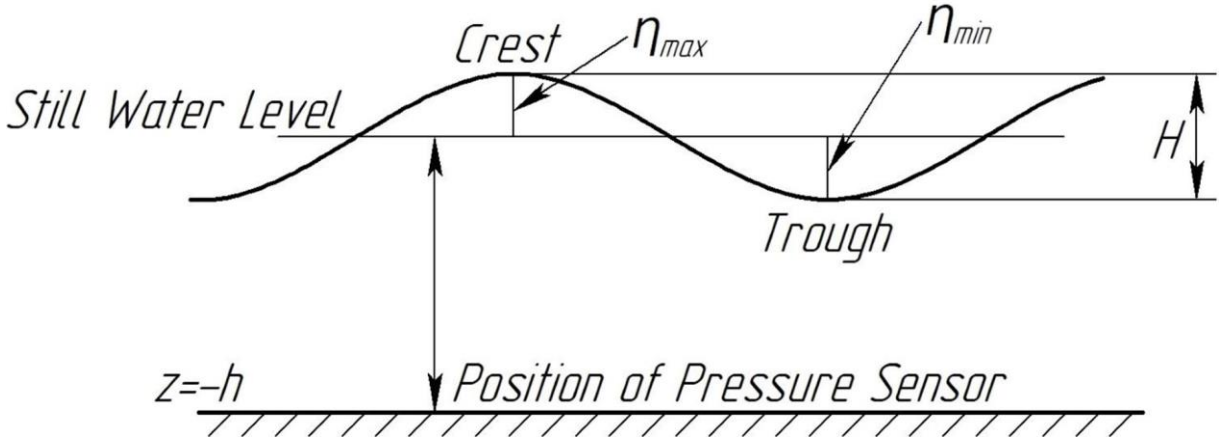

Figure 7. Schematic diagram of wave height from a pressure measurement.

Thus, Wave Height can be evaluated from Eq. 26.

$$H = (\eta_{max} - \eta_{min}) = (P_{max} - P_{min}) \frac{\cosh(kh)}{\rho g} \qquad (26)$$

As seen in the above equation, wave height is the function of wavenumber, $k = \frac{2\pi}{L}$ and its function of wavelength. Wave height and wave period were obtained by using the Rayleigh distribution and the zero-up crossing analysis method. Based on the results from the previous section, the Newton Raphson numerical method is the best equation that can be used to solve the dispersion relation with the smallest error. Thus, the wavelengthv was obtained vby using a dispersion relationship that was solved by using the Newton Raphson numerical method. Two Matlab codes were built to avoid manual calculation and get an accurate value of wave height, as seen in the following Figures 8, 9, and 10, and were evaluated at three different wave frequencies. The significant wave height (H_s) obtained and is defined as the average height of the highest one-third of waves in a wave spectrum. The significant wave height is very often considered as the design wave. The comparison between the results was evaluated based on pressure measurement and the analyzed images captured using the PIV technique can be seen in the discussion section.

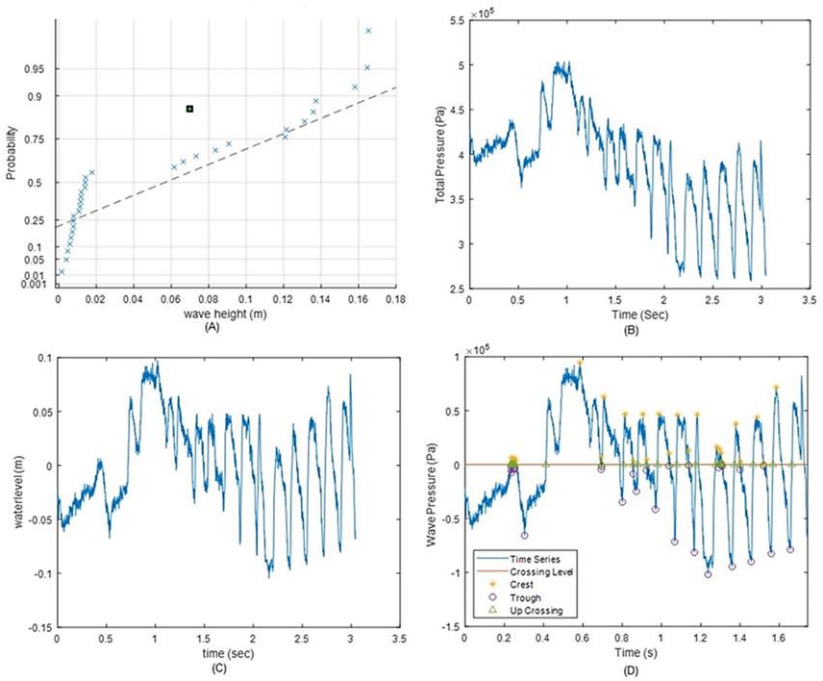

Figure 8. Wave record with a period of T=0.4771 Sec. A: The Rayleigh distribution of the pressure sensor, B: Total pressure caused by hydrostatic pressure and wave pressure, C: Wave surface profile $(\boldsymbol{\eta})$, D: Zero -up crossing applying on dynamic pressure caused by the wave.

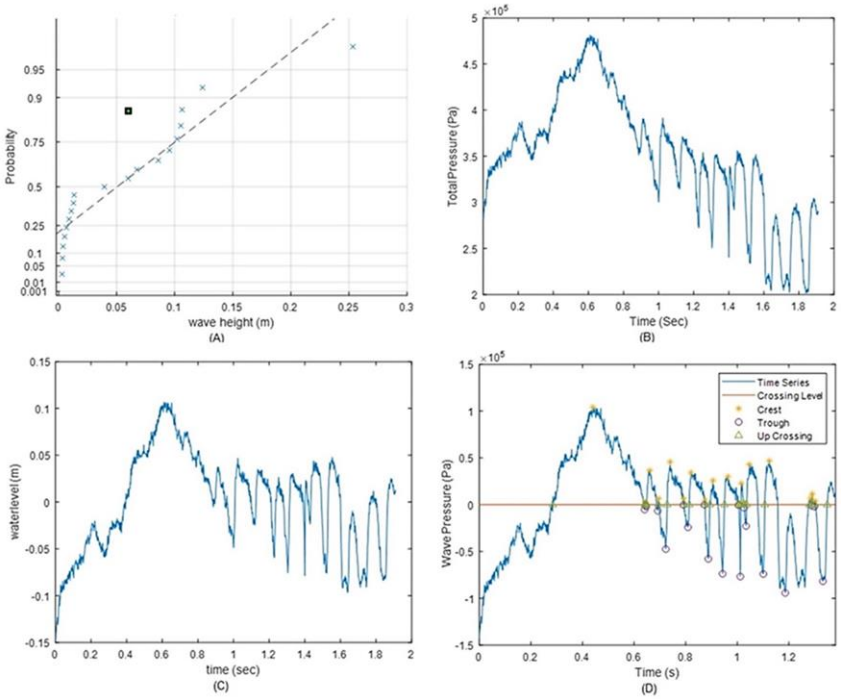

Figure 9. Wave record with a period of T=0.5576 Sec. A: The Rayleigh distribution of the pressure sensor, B: Total pressure caused by hydrostatic pressure and wave pressure, C: Wave surface profile $(\boldsymbol{\eta})$, D: Zero -up crossing applying on dynamic pressure caused by the wave.

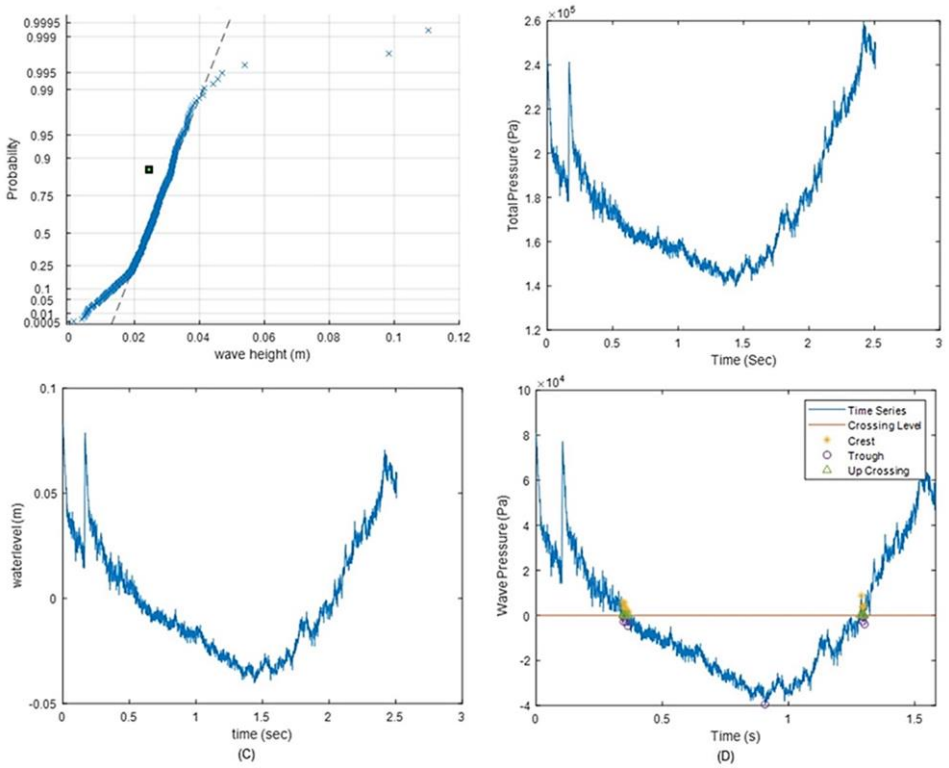

Figure 10. Wave record with a period of T=0.9585 Sec. A: The Rayleigh distribution of the pressure sensor, B: Total pressure caused by hydrostatic pressure and wave pressure, C: Wave surface profile $(\boldsymbol{\eta})$, D: Zero -up crossing applying on dynamic pressure caused by the wave.

4.3. Based on PIV image (image processing)

4.3.1. PIV technique setup

The PIV setup is shown in Figure 11. A big sky double pulsed Nd: YAG (Neodymium-Doped Yttrium Aluminum Garnet) laser of wavelength 532 nm and 200 mJ/Pulse with the maximum repetition rate of 15 Hz per laser head was used to provide illumination of the seeding particles. The laser sheet adjustment is the most important step in PIV setup to obtain highly accurate results and safety issues. This was done using orange light-sensitive paper. That paper was placed in the front of the laser beam source in the middle of the flume tank (test section, the location where the laser sheet should be generated). The laser beam source was performed with a lower laser energy limit and was visible in the dark ambient light condition to ensure safety. The two laser beams sources should leave marks on the orange paper. One mark was found on the orange paper, which means two laser beams are hitting at the same point (LaVision GmbH, 2016). The laser beam source was directed from above the flume tank towards the middle of the water surface using a 45° dielectric mirror, then a cylindrical lens was used to convert the laser beam into the laser sheet with a thickness is about 2 mm.

The laser sheet was generated to be perpendicular to the water surface and parallel to the sidewall of the flume tank. The laser sheet was slightly inclined at a 6° downwind from the middle of the flume tank. LaVision charged coupled device (CCD)Imager Pro X 2m camera was used. The camera resolution is 1600 x 1200 pixels with a bit depth of 14 bit, and the pixel size is 7.4μm. The camera has a double exposure feature with an interframe time down to 100 ns, and the frame rate is 30 fps at full resolution. The camera is fitted with an adapter to connect it with a NIKON AF NIKKOR zoom lens (50 mm 1:1.8 D), which means the focal length is 50 mm, and the f- stop number is 1.8. Camera alignment is a critical issue that can affect the accuracy of the measurement. Thus, the CCD camera should be set with the optical axis perpendicular to the laser sheet. The misalignment between a CCD camera and the laser sheet produces a bias in the measurements (Kompenhans et al., 2002; Raffel et al., 1996; Scarano, 2013). The camera was mounted in the front of the flume tank with a 6° inclined angle from the perpendicular axis, as shown in Figure 12.

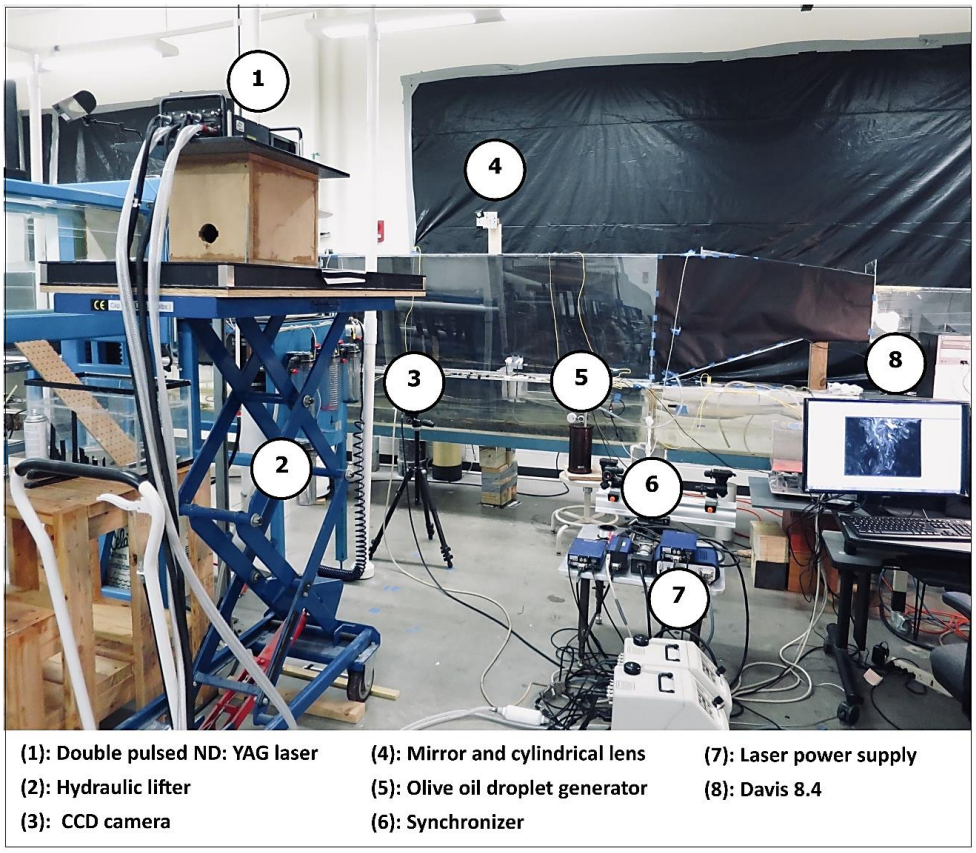

Figure 11. Schematic diagram of the PIV setup used in this experiment.

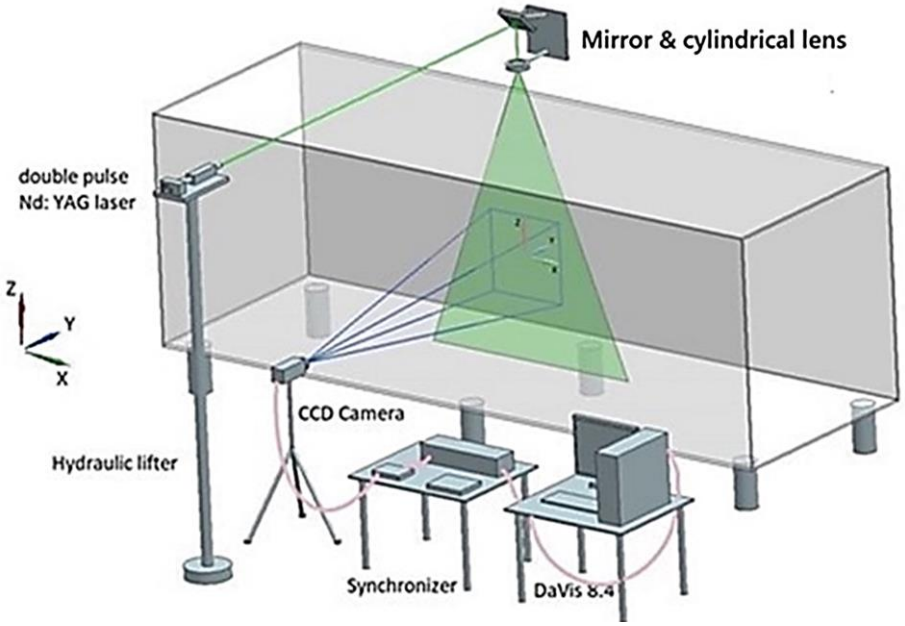

Figure 12. Experimental setup of PIV.

The calibration algorithm in Davis (8.4) was used to calibrate the CCD camera to make sure the camera was arranged perpendicular to the laser sheet. HGS-10 hollow glass sphere with diameter 10μm and the density of $1.10 \pm 0.05\ g/cm^3$ from Dantec was used as the seeding particles, and it is known as the best particles for water flow (Scarano, 2013). A synchronizer is a control unit that is used to provide external triggers for the CCD camera and the two pulsed laser sources. The synchronizer can be used to control the delay time between the two pulsed laser beams, which is known as synchronizer separation time Δt, and the firing of two pulsed laser beams relative to CCD camera exposure. All these steps were controlled by Davis 8.4 from LaVision. The separation time Δt is a critical parameter used to evaluate velocity components of the flow. Determining the optimal pulse separation time Δt of the two-laser beam depends on the flow behavior and can be set manually by the user or automatically by Davis 8.4 based on the wanted particle shift.

This experiment was done at the fluid dynamic laboratory at WMU, and the laboratory was completely dark when the PIV images were taken to reduce the illumination variability. This was done by covering the backside of the Acrylic Plexiglass flume tank with black paper, covering all lab windows with black plastic sheets, and turning off the light inside the lab.

4.3.2. Analyzed images captures using the PIV technique

The wave images at three different frequencies were captured using PIV techniques, as was explained above. As was illustrated before, the main objective of this method is to obtain wave height and wavelength. Due to space limitations at the front of the wave in the test section, it was not able to increase the field of view and capture a full wavelength. Thus, Matlab code was built to create a full wavelength from many successive PIV images. The Canny edge detection algorithm technique with the constant threshold value was used to detect the edge of the wave (water surface elevation) (Kamanga, 2017; Lee et al., 1987; Marques, 2011; Marr & Hildreth, 1980; Shokhan, 2014). Also, by using Matlab, the minimum points (trough) and maximum point (crest) at the one full wavelength were determined. Then, the values of wavelength and wave height were obtained by using the definition of wavelength (distance between two successive troughs) and wave height (the distance between crest and trough). Finally, to ensure that accurate results were evaluated, the final value of wavelength and wave height was calculated by taking the average of ten values obtained from ten trials, as is shown in Figure 13.

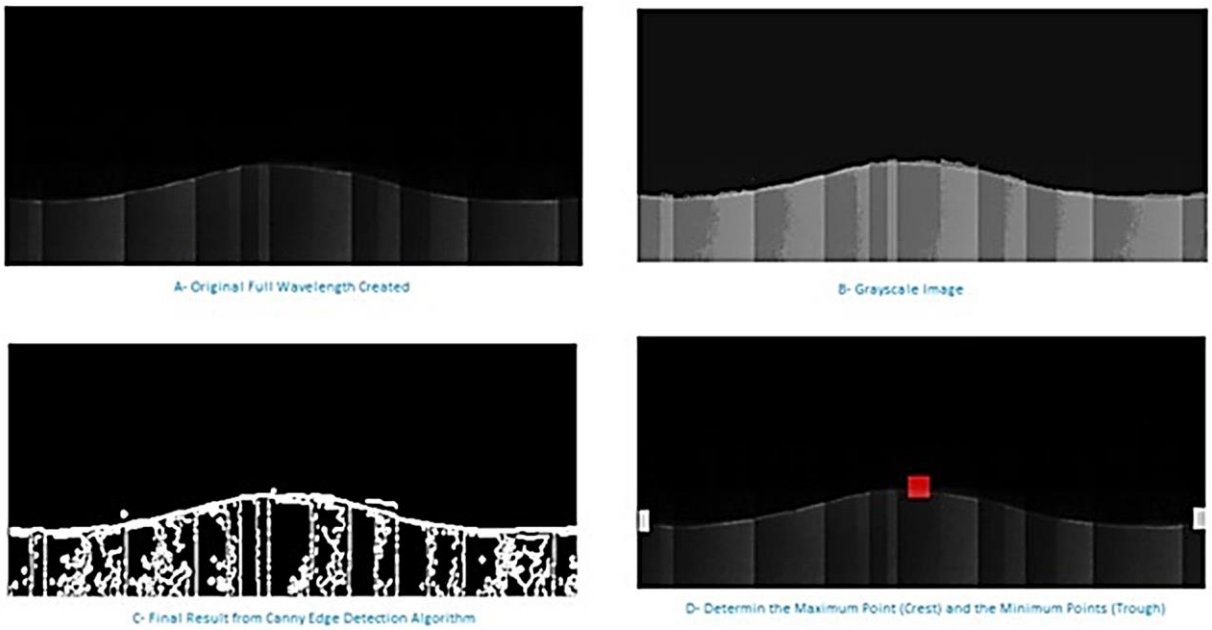

Figure 13. The procedure of water surface detection: a- Original full wavelength created b- Grayscale image
c- Result from canny edge detection with constant threshold value
d- Determine the maximum point (crest) and the minimum points (trough).

5. Results and discussion

The current study investigates the performance of three different methods which could be employed to measure the characteristics (specifically wave height and wavelength) of the intermediate water gravity waves generated mechanically in the flume tank. The methods proposed include making use of the wavemaker transfer function, the wave-induced pressure, and PIV-based image processing to obtain the wave characteristics. Table 2 shows the value of the wavelength and wave height obtained from analyzing the PIV images as explained earlier in section 4.2.3.

Dispersion theory was used to evaluate wavelength then substituted back into wavemaker transfer function Equation 21 to get the value of wave height. Wavelength cannot be directly solved for a given set of wave period (T) or still water depth(h) from dispersion theory. Thus, to get the value of wavelength, it should be found by iteration. In this study, four numerical methods were used to get wavelength, and the percentage of error was calculated relative to the value of wavelength and wave height obtained by analyzing PIV images that were considered as the true value of the wave measurements. The four most common numerical methods found in the literature that are used to evaluate wavelength are Newton Raphson method, Hunt method, Eckart method, and Approximation method. As shown below in Table 3, the smallest deviation was given by using the Newton Raphson method, followed by the Hunt Method.

Table 2. The wave characteristic calculated based on the PIV images analysis.

Parameters, m	Period T= 0.4771 sec	Period T= 0.5576 sec	Period T= 0.9585 sec
Wavelength	0.357989	0.474643	1.083282
Wave height	0.069296	0.059355	0.02672

Table 3. The wave characteristic calculated based on the flap wavemaker theory.

A: - Wave period (T)= 0.4771 sec, wavelength (L)=0.357989 m, Wave height(H)=0.069296 m

Type of method	Wavelength was calculated using dispersion relation, m	Percent of Error % (L)	The wave height was calculated using transfer function of flap wavemaker, m	Percent of Error % (H)
Newton Raphson	0.358	0.0272	0.07310	5.489
Hunt	0.357	0.1918	0.07316	5.576
Eckart	0.359	0.2207	0.0730	5.345
Approximation	0.355	0.9575	0.07343	5.966

B: -Wave period (T)= 0.5576 sec, wavelength (L)=0.474643 m, Wave height(H)=0.059355 m

Type of method	Wavelength was calculated using dispersion relation, m	Percent of Error % (L)	The wave height was calculated using transfer function of flap wavemaker, m	Percent of Error % (H)
Newton Raphson	0.475	0.0264	0.06183	4.169
Hunt	0.474	0.1495	0.06191	4.3046
Eckart	0.480	1.0274	0.06139	3.4285
Approximation	0.468	1.3379	0.06244	5.198

C: - Wave Period (T)= 0.9585 sec, Wavelength (L)=1.083282 m, Wave Height(H)= 0.02672 m

Type of method	Wavelength was calculated using dispersion relation, m	Percent of Error % (L)	The wave height was calculated using transfer function of flap wavemaker, m	Percent of Error % (H)
Newton Raphson	1.084	0.0342	0.02824	5.6886
Hunt	1.0836	0.0311	0.02824	5.6886
Eckart	1.140	5.2580	0.0267	0.07485
Approximation	1.093	0.8714	0.0279	4.2723

The experimental data recorded using Honeywell pressure sensor were analyzed using Matlab software. Two Matlab codes were built to avoid manual calculation and get an accurate value of wave height, as shown in Figures 8 through 10, and were evaluated at three different wave frequencies. Then, the wavelength was obtained by using a dispersion relationship that was solved by using the Newton Raphson numerical method. The results obtained from pressure measurements and comparing these results with the results evaluated based on analyzed PIV images are summarized in Table 4.

Noteworthy to notice that the Newton Raphson numerical method is the best equation that can be used to solve the dispersion relation with the smallest deviation compared to values obtained based on analyzing PIV images were considered as the true value of wavelength and wave height. The percentage of deviation of the values produced by using the Newton Raphson method obtained based on the pressure measurements were ranging between (0.0264-0.0342) percent for wavelength and (4.169-5.6886) percent for wave height. Whereas values obtained based on the wavemaker transfer function were ranging between (0.0244-1.2128) percent for wavelength and (0.8716-8.683) percent for the wave height.

6. Conclusion

Waves were generated mechanically by a flap-type bottom-hinged paddle mounted at one end of the wave flume tank, which travels down the trough and is expected to dissipate smoothly on the slope of the beach, or it can be called a wave absorber. This experiment employed three different methods to obtain the characteristic wave parameters like wave period, wavelength, and wave height: based on the theory of flap-wavemaker transfer function, pressure measurements that were evaluated from the Honeywell pressure sensor readings and based on PIV images that were analyzed using Matlab software and the concept of canny edge detections. This experiment was focused on getting the direct value of wavelength and wave height and eliminating the errors that may produce by solving dispersion relation theory by one of the numerical methods. Then, the comparison between these methods was made and the percentage of error was calculated to evaluate the performance of these methods to get accurate wave measurements. Pressure measurements-based methods are conventional methods, point measurements, intrusive, and sometimes it is very hard to set up. At the same time, the transfer function of the flap wavemaker is valid only when the frequency of the flap wavemaker is the same as the frequency of the regular waves generated inside the wave flume tank. The PIV technique can be applied easily in the area of interest, reduces spatial sampling cost, and is valid for regular and irregular waves. The accuracy of the results obtained by analyzing the PIV image is strongly affected by the quality of PIV images, the performance of edge detection algorithms used, and the PIV setup (seeding, CCD camera, and camera calibration) (Viriyakijja & Chinnarasri, 2015). It is noteworthy to observe that the accurate value of wavelength and wave height obtained based on the pressure measurements and wavemaker transfer function are strongly dependent on the numerical method that should be used to solve the dispersion theory. Noteworthy to notice the most accurate results can be evaluated by employing the Newton Raphson numerical method.

Table 4. The wave characteristic calculated based on pressure measurement.

Type of method	Wavelength was calculated using dispersion relation, m	Percent of Error % (L)	The wave height was calculated using Pressure Measurement, m	Percent of Error % (H)
Newton Raphson	0.354	1.2128	0.0699	0.8716

B: -Wave Period (T)= 0.5576 sec, Wavelength (L)=0.474643 m, Wave Height(H)=0.059355 m

Type of method	Wavelength was calculated using dispersion relation, m	Percent of Error % (L)	The wave height was calculated using Pressure Measurement, m	Percent of Error % (H)
Newton Raphson	0.478	0.7984	0.06183	4.169

C: - Wave Period (T)= 0.9585 sec, Wavelength (L)=1.083282 m, Wave Height(H)= 0.02672

Type of method	Wavelength was calculated using dispersion relation, m	Percent of Error % (L)	The wave height was calculated using Pressure Measurement, m	Percent of Error % (H)
Newton Raphson	1.083	0.0041	0.0244	8.683

Conflict of interest

The authors have no conflict of interest to declare.

Funding

The authors received no specific funding for this work.

References.

Andersen, T. L., & Frigaard, P. (2011). Lecture Notes for the Course in Water Wave Mechanics, Aalborg, Denmark: *Department of Civil Engineering, Aalborg University.DCE Lectur* no. 24, P. 116.

Blenkinsopp, C. E., Mole, M. A., Turner, I. L., & Peirson, W. L. (2010), Measurements of the time-varying free-surface profile across the swash zone obtained using an industrial LIDAR. *Coastal Engineering*, *57*(11–12), 1059–1065. https://doi.org/10.1016/j.coastaleng.2010.07.001

Blenkinsopp, Chris E., Turner, I. L., Allis, M. J., Peirson, W. L., & Garden, L. E. (2012), Application of LiDAR technology for measurement of time-varying free-surface profiles in a laboratory wave flume. *Coastal Engineering*, *68*(October 2012), 1–5. https://doi.org/10.1016/j.coastaleng.2012.04.006

Bonmarin, P., Rochefort, R., & Bourguel, M. (1989), Experiments in Fluids Surface wave profile measurement by image analysis. *Experiments in Fluids*, *24*(1), 17–24. https://doi.org/10.1007/BF00226592

Dean, R. G., & Dalrymple, R. A. (1991). *Water wave mechanics for engineers and scientists* (Vol. 2). world scientific publishing company.

Douglas, S., Cornett, A., & Nistor, I., (2020), Image-based measurement of wave interactions with rubble mound breakwaters. *Journal of Marine Science and Engineering*, *8*(472), 1–16. https://doi.org/10.3390/jmse8060472

Erikson, L. H., & Hanson, H., (2005), A method to extract wave tank data using video imagery and its comparison to conventional data collection techniques. *Computers & Geosciences*, *31*(3), 371–384. https://doi.org/10.1016/j.cageo.2004.10.006

Escudero, M., Hernández-Fontes, J. V., Hernández, I. D., & Mendoza, E., (2021), Virtual level analysis applied to wave flume experiments: The case of waves-cubipod homogeneous low-crested structure interaction. *Journal of Marine Science and Engineering*, *9*(230), 1–18. https://doi.org/10.3390/jmse9020230

Hernández-Fontes, J. V., Hernández, I. D., Silva, R., Mendoza, E., & Esperança, P. T. (2020). A simplified and open-source approach for multiple-valued water surface measurements in 2D hydrodynamic experiments. *Journal of the Brazilian Society of Mechanical Sciences and Engineering*, *42*(12), 623. https://doi.org/10.1007/s40430-020-02702-x

Hernández, I. D., Hernández-Fontes, J. V., Vitola, M. A., Silva, M. C., & Esperança, P. T. T., (2018), Water elevation measurements using binary image analysis for 2D hydrodynamic experiments. *Ocean Engineering*, *157*, 325–338. https://doi.org/10.1016/j.oceaneng.2018.03.063

Hwung, H. H., Kuo, C. A., & Chien, C. H. (2009). Water surface level profile estimation by image analysis with varying overhead camera posture angle. *Measurement Science and Technology*, *20*(7), 075104. https://dx.doi.org/10.1088/0957-0233/20/7/075104

Iglesias, G., Ibáñez, O., Castro, A., Rabuñal, J. R., & Dorado, J., (2009), Computer vision applied to wave flume measurements. *Ocean Engineering*, *36*(14), 1073–1079. https://doi.org/10.1016/j.oceaneng.2009.06.012

Kamanga, I., (2017), An Adaptive Approach to Improve Canny Method for Edge Det ection. *International Journal of Science and Research*, *6*(6), 164–168.

Kompenhans, J., Arnott, A., Agocs, A., Gilliot, A., Arnott, A., & Monnier, J. C. (2002). Application of particle image velocimetry for the investigation of high speed flow fields. *West East High Speed Flow Fields*.

LaVision GmbH. (216). LaVision. LaVision GmbH. Retrieved https://www.lavision.de/en/index.php

Lee, D. Y., & Wang, H. (1984). Measurement of surface waves from subsurface gage. In *Coastal Engineering 1984* (pp. 271-286). https://doi.org/10.1061/9780872624382.020

Lee, J. S. J., Haralick, R. M., & Shapiro, L. G. (1987), Morphologic Edge Detection. *IEEE Journal on Robotics and Automation*, *3*(2), 142–156. https://doi.org/10.1109/JRA.1987.1087088

Li, Q., Zhao, M., Tang, S., Sun, S., & Wu, J. (1993), Two-dimensional scanning laser slope gauge: measurements of ocean-ripple structures. *Applied Optics*, *32*(24), 4590–4597. https://doi.org/10.1364/ao.32.004590

Liu, H. T., Katsaros, K. B., & Weissman, M. A. (1982), Dynamic response of thin-wire wave gauges. *Journal of Geophysical Research*, *87*(08), 5686–5698. https://doi.org/10.1029/JC087iC08p05686

Marques, O. (2011). *Practical image and video processing using MATLAB*. John Wiley & Sons.

Marr, D., & Hildreth, E. (1980), Theory of edge detection. *Proceedings of the Royal Society of London. Series B, Biological Sciences*, *207*(1167), 187–217. https://doi.org/10.1098/rspb.1980.0020

Mukto, M. A., Atmane, M. A., & Loewen, M. R. (2007), A particle-image based wave profile measurement technique. *Experiments in Fluids*, *42*(January 2007), 131–142. https://doi.org/10.1007/s00348-006-0226-6

Payne, G. S., Richon, J.-B., Ingram, D., & Spinneken, J. (2009), Development and preliminary assessment of an optical wave gauge. *8th European Wave and Tidal Energy Conference (EWTEC 2009),Uppsala, Sweden*, *September 7*, *2009*, 160–167.

Raffel, M., Höfer, H., Kost, F., Willert, C., & Kompenhans, J. (1996). Experimental aspects of PIV measurements of transonic flow fields and their benefit for the optimization of gas turbines. In *Proc. Eighth International Symposium on Applications of Laser Techniques to Fluid Mechanics* (pp. 28-1). https://elib.dlr.de/37469/

Saincher, S., & Banerjee, J. (2015), Design of a numerical wave tank and wave flume for low steepness waves in deep and intermediate water. *Procedia Engineering*, *116*(1), 221–228. https://doi.org/10.1016/j.proeng.2015.08.394

Scarano, F. (2013), Tomographic PIV: Principles and practice. *Measurement Science and Technology*, *24*(1), 012001–012028. https://doi.org/10.1088/09570233/24/1/012001

Shokhan, M. H. (2014). An efficient approach for improving canny edge detection algorithm. *International Journal of Advances in Engineering & Technology*, *7*(1), 59.

Siddiqui, M. H. K., Loewen, M. R., Richardson, C., Asher, W. E., and Jessup, A. T. (2001), Simultaneous particle image velocimetry and infrared imagery of microscale breaking waves. *Physics of Fluids*, *13*(7), 1891–1903. https://doi.org/10.1063/1.1375144

Trujillo, A. P., & Thurman, H. V. (2011). *Essentials of Oceanography*, Glenview, IL, USA: Pearson Prentice Hall, 2011, P. 551.

Viriyakijja, K., & Chinnarasri, C. (2015). Wave Flume Measurement Using Image Analysis. *Aquatic Procedia*, *4*(ICWRCOE 2015), 522–531. https://doi.org/10.1016/j.aqpro.2015.02.068

Vousdoukas, M. I., Kirupakaramoorthy, T., Oumeraci, H., de la Torre, M., Wübbold, F., Wagner, B., & Schimmels, S. (2014), The role of combined laser scanning and video techniques in monitoring wave-by-wave swash zone processes. *Coastal Engineering*, *83*, 150–165. https://doi.org/10.1016/j.coastaleng.2013.10.013

Wang, C., Chen, P., & Liao, C. (2012), Application of CCD cameras as a versatile measurement tool for flume tank. *Ocean Engineering Journal*, *42*, 71–82. https://doi.org/10.1016/j.oceaneng.2012.01.020

Yao, A., & Wu, C. H. (2005), An automated image-based technique for tracking sequential surface wave profiles. *Ocean Engineering*, *32*(2), 157–173. https://doi.org/10.1016/j.oceaneng.2004.07.004

Zarruk, G. A. (2005), Measurement of free surface deformation in PIV images. *Measurement Science and Technology*, *16*(October), 1970–1975. https://doi.org/10.1088/0957-0233/16/10/012